Flexible Motion Planning for Object Manipulation in Cluttered Scenes

Marco Costanzo, Giuseppe De Maria, Gaetano Lettera, Ciro Natale and Salvatore Pirozzi
Dipartimento di Ingegneria, Università degli Studi della Campania Luigi Vanvitelli, Via Roma 29, Aversa, Italy

Keywords: Reactive Robot Control, Robot Motion Planning, Object Recognition, Obstacle Avoidance.

Abstract: The work implements a new real-time flexible motion planning method used for reactive object manipulation in pick and place tasks typical of in-store logistics scenarios such as shelf replenishment of retail stores. This method uses a new hybrid pipeline to recognize and localize an object observed through a depth camera, by integrating and optimizing state of the art techniques. The proposed algorithm guarantees recognition robustness and localization accuracy. The desired object is then manipulated. The motion planner, based on the obstacles detected in the scene, plans a collision-free path towards the target pose. The planned trajectory optimizes a cost function that reflects the best solution among those available and produces natural and smooth path through a smart IK constrained solution which avoids robot unnecessary reconfigurations. A reactive control based on distributed proximity sensors is finally adopted to locally modify the planned trajectory in real time to avoid collisions with uncertain or dynamic obstacles. Experimental results in a supermarket scenario populated with cluttered obstacles demonstrate smoothness of the robot motions and reactive capabilities in a typical fetch and carry task.

1 INTRODUCTION

Nowadays, robotic systems are used in unstructured environments where motions cannot be preprogrammed. The state-of-the-art (SoA) motion planners are based on off-line sample-based algorithms, such as Rapidly-exploring Random Tree (RRT) (Kuffner and LaValle, 2000), Probabilistic RoadMap (PRM) (Kavraki et al., 1996), Expansive Spaces Tree (EST) (Phillips et al., 2004), Kinematic Planning by Interior-Exterior Cell Exploration (KPIECE) (Şucan and Kavraki, 2009), which are all tree-based planners. They are theoretically consistent but difficult to tune and to effectively use in practice without a specific customization for the considered application. Moreover, their random nature often causes unnatural trajectories. These planners work in joint space so they need an IK solution as input for the target pose. The most used Inverse Kinematics (IK) solver is Kinematic and Dynamic Solver (KDL) (Khokar et al., 2015), which is based on Newton's method with some random jumps. However, careless use of IK solvers can produce unneeded robot reconfigurations.

Another challenge for robots acting in unstructured environments is the object recognition and localization task. The SoA techniques propose pipelines too application-tailored, which are difficult to generalize. Some local descriptors, such as Fast Point Feature Histograms (FPFH) (Rusu et al., 2009) or Signature of Histograms of OrienTations (SHOT) (Tombari et al., 2010), work well when only few objects are in the scene, far enough from each other and not similar. On the other hand, the main limit of global descriptors, such as Viewpoint Feature Histogram (VFH) (Rusu et al., 2010), is the possible presence of partial occlusions.

The technologies described so far for object recognition and localization and for robot motion planning are the key enablers for the robotization of many processes typical of the logistic and intra-logistic application fields. With reference to the retail market, both in the distributions centers and in the supermarket stores, a large number of single items per time unit have to be fetched and carried from a place to another, e.g., in a store, from a trolley to a shelving unit. Robots have not entered yet into such a context for their limited manipulation abilities in terms of number and type of objects that they can safely grasp and handle. Safe grasping is not the only challenge but also motion planning is quite a difficult task for a robot. Usually, many different items have to be fetched from a tray to a shelf, where other objects are already present and can be misplaced and where the

Costanzo, M., Maria, G., Lettera, G., Natale, C. and Pirozzi, S.
Flexible Motion Planning for Object Manipulation in Cluttered Scenes.
DOI: 10.5220/0006848701100121
In *Proceedings of the 15th International Conference on Informatics in Control, Automation and Robotics (ICINCO 2018) - Volume 2*, pages 110-121
ISBN: 978-989-758-321-6

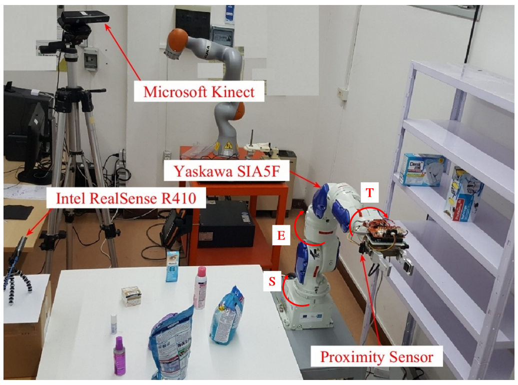

Figure 1: Experimental set-up.

items have to be placed in usually narrow spaces and very close to each other.

This paper tries to overcome the discussed SoA limitations. The main contributions can be summarized as follows. A novel hybrid pipeline for object recognition and localization is proposed to achieve more reliability and the accuracy needed for a correct grasp. The considered task consists in detecting an assigned object among many placed on a trolley tray, picking it and placing it on a shelf. Therefore, given the model of the object, the scene is segmented and the clusters identified, then the model is compared to each cluster and the association depends not only on the comparison of the descriptors selected for modeling the object and the cluster but also on the alignment process itself. An obvious drawback of this approach is the longer computational time, that is the price to pay for a higher success rate. A second contribution consists in a procedure that ensures a planned motion with no unnecessary arm. This is achieved by careful use of a constrained IK solver to look for a joint configuration corresponding to the target pose as close as possible to the initial one. Last but not least, this paper does not limit to a simple “plan and act” approach, which suffers from uncertainties and dynamic changes in the scene. The robot is endowed with a reactive control capability that usefully exploits distributed proximity sensors providing information on the actual location of the obstacles near the end effector, an idea used also by (Nakhaeinia et al., 2018). A simple control algorithm is proposed to locally modify directly the planned trajectory in the joint space so as to ensure avoidance of unexpected or uncertainly placed obstacles. To demonstrate the effectiveness of the new approaches proposed in the paper, a number of experiments have been conducted on a fairly large object set and with an industrial robot in a setting representative of a shelf refilling task of a supermarket scenario (Figure 1).

2 OBJECT RECOGNITION AND LOCALIZATION

This section describes the proposed object recognition and 6D localization algorithm, with special emphasis on the hybrid pipeline. The algorithm processes information obtained from the point clouds acquired by the sensory system described in Section 2.1. The aim is to align point clouds using a model-based approach, which compares object geometric information of some objects, placed on a planar surface, with those of the given 3D target model.

2.1 Sensory System

A structured light sensor has been adopted for creating depth maps. The Intel RealSense R410 camera has been used as vision device for both object recognition and localization (see Figure 1). It uses an IR emitter to project a light pattern and an IR sensor to detect the deformations in the projected pattern for resolving the depth, without any RGB information. The R410 maximum resolution is 1280x720. After selection of the fixed camera position according to the criteria explained in Section 2.3.4, a calibration procedure has been required to estimate both the intrinsic and extrinsic parameters of the camera. In particular, a simple procedure has been developed to obtain the homogeneous transformation matrix from the camera frame to the robot frame, i.e., the T_{camera}^{robot} matrix. The procedure generates two transformation matrices, by using a third coordinate frame on a fixed object corner: T_{object}^{robot}, which expresses the pose of the object frame with respect to the robot base frame; T_{object}^{camera}, which expresses the pose of the object frame with respect to the camera frame. By combining them, the recognized object pose can be expressed relatively to the robot frame, to allow the robot to manipulate it.

2.2 Object Set and Models

The set of objects used for the training process is shown in Figure 2. Since no 3D models are directly available for the selected objects, many of them have been reconstructed automatically using the Intel sensor and the ReconstructMe online software. For the objects of simple geometry, a CAD model has been directly drawn using a CAD program. Views of the resulting 3D models can be seen in Figure 3. Note that ReconstructMe is not able to distinguish the liquid inside the transparent objects or to track thin or polished items during the rotation required by the modeling procedure. Therefore, such kind of objects have been eventually excluded form the considered set (those

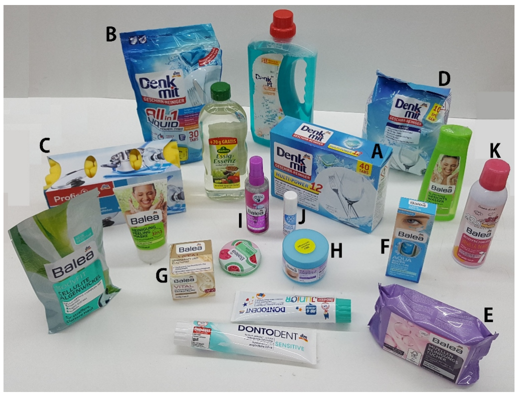

Figure 2: Object training set.

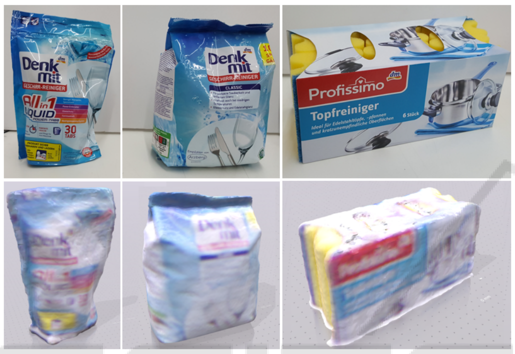

Figure 3: Some reconstructed 3D models.

not labelled in Figure 2). All the models are finally converted into Point Cloud Data (*.pcd*) files, to be elaborated by the Point Cloud Library (PCL) (Rusu and Cousins, 2011). A complete point cloud model could have regions that are doubled in overlapping areas, due to small registration errors, and holes, due to scanning surfaces that did not return any distance measurements (e.g., shiny or metallic objects). Therefore, the obtained point clouds are then filtered with the *Moving Least Squares (MLS)*, which is a widely used technique for approximating scattered data using smooth functions.

2.3 Comparison Among Existing Algorithms

One of the main goals of 3D data processing is about matching regions. This process generally happens between two point sets S_1 and S_2, which can be compared through a method based on the *descriptor* notion. Descriptors can be defined like the structures that contain useful information to summarize the points of a point cloud and in this work they are used to search correspondences between an object model and scene points. As described in (Aldoma et al., 2012), depending on the way they represent the information, 3D descriptors can be divided into two main categories: Signatures or Histograms. The descriptor of each category, depending on the extension of the point cloud to which it is applied, can be local or global. Descriptors of single objects and scene areas belong to the local category, while global descriptors describe the scene using all pixels of the image. On this distinction, the state of the art advises to follow two possible pipelines, depending on the case study, shown in Figure 4. However, many limitations have been found to generalize the recognition and localization tasks and that is why a new hybrid approach has been adopted.

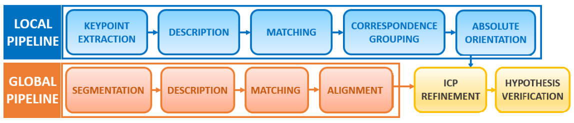

Figure 4: The SoA local and global pipelines.

2.3.1 Local Pipeline

3D local descriptors work on specific points, called *keypoints*. They contain information from a neighborhood, which is usually determined by selecting points within a radius from the center point. The description of a complete object consists in associating each point with a descriptor of the local geometry of the same point. Referring to Figure 4, the main phases of a local pipeline are the first three:

1. Keypoint Extraction: They represent points of interest which are stable, characteristic or distinctive. However, tests carried out with extracted edges, a typical keypoint criterion, did not produce satisfactory results in cluttered scenes.

2. Description: This second step associates the descriptors to the keypoints. As above, a common trait of all local descriptors is the definition of a local support used to determine the subset of neighboring points around each keypoint that will be used to compute its description: the best choice for the *support size* was about 0.02 m. Intuitively, it is understood how the support size may be defined either in terms of length, or in terms of the number of neighbors. During experimental tests, the choice has been obviously a trade-off since a fixed number of neighbors means that histograms will have the same total magnitude but will also be more susceptible to differences in point density. This means that the radius parameter is somewhat robust but its size does need to be tuned for the specific class of object that is being recognized: if the size is too small, the descriptor will describe basic features like planes and corners and will lose its ability to discriminate. On the other hand, if the radius is too large it will contain information from much of the background and it will not match to anything.

3. Matching: Then, a pair of points (p_m, p_s), with p_m point of the model and p_s point of the scene, can be defined a *correspondence* if their Euclidean distance is below a certain threshold, chosen a priori by the user. To make the comparison step even more efficient, it has been applied a particular comparison pattern on the matching neighborhoods found, called the Fast Library Approximate Nearest Neighbors (FLANN) algorithm (Muja and Lowe, 2009). Even in this step, searching the optimal threshold value is crucial: a too low value generates too many possible combinations in the total scene; a too high value makes the matching algorithm too greedy. Searching a unique value for different scenes and the same model was impossible.

2.3.2 Global Pipeline

Global descriptors are high-dimensional representations of the geometric features of an object. Their use is similar to that of local descriptors but, due to high computational cost, they are generally calculated after a 3D segmentation. Even if the global sequence of phases is similar to that of the local pipeline, there is a deep difference: the object is now described in its entirety and not only through some of its points, without keypoints. With reference to Figure 4, the main steps of a global pipeline are:

1. Segmentation: Segmentation is a well-researched topic and several techniques exist (Bergstrom et al., 2011), (Mishra and Aloimonos, 2011), (Comaniciu and Meer, 2002). It is needed to identify the various objects that are part of the scene. Different techniques can be used, such as the *Differences between point clouds*, which is a background subtraction method, the *Euclidean pooling* method that splits point clouds in a series of subgroups distant among each other a given amount (similar to the k-mean segmentation), *Extraction of polygons and solids*, which detects a subset of points that resemble a geometrical primitive (cylinder, sphere, ...), *Segmentation of normal* method, based on the extraction of surfaces whose normals have a particular direction.

2. Description: The output of scene segmentation is a set of clusters, supposedly each representing a single object of the scene. The shape and geometry of each of these objects are described by means of a proper global descriptor and represented by a single histogram. It is obvious that the obtained descriptor is highly affected by partial occlusions, hence the following matching phase will likely fail in such cases.

3. Matching: In all cases, the histogram is independently compared against those obtained in the training stage, getting the best N matches. Matches are not pairs of points as in the case of local descriptors, but the set of N model views that can be superimposed on the scene by applying a transformation. Typically, the histogram matching is done using FLANN by means of a brute force search, and the distance between histograms is computed using the L_1 metric.

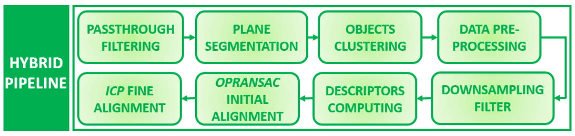

Figure 5: The proposed hybrid pipeline.

2.3.3 Hybrid Pipeline

Taking into account that, in the considered application, only geometric information about the objects is available (no visual features are used), the scene is usually large and affected by partial occlusions, similar objects are close to each other, local and global SoA pipelines are not suitable for the limitations discussed above. The proposed algorithm extracts the most generalizable steps of each standard SoA pipeline, that means the global segmentation and the local descriptor robustness, as shown in Figure 5. Moreover, a new approach is introduced: unlike the SoA pipeline that provides the matching phase and the alignment phase as two separated steps, the proposed algorithm takes the two phases in one step. It also optimizes a critical parameter to be more efficient and robust than the traditional approach. The initial coarse alignment provided by the RANdom SAmple Consensus (RANSAC) method (Papazov and Burschka, 2011) is finally refined by the Iterative Closest Point (ICP) method (Rusinkiewicz and Levoy, 2001). The output of the proposed algorithm is the 6D pose of the recognized object. The hybrid pipeline is divided into 8 steps:

1. PassThrough Filtering. A series of filters available in the PCL library are applied to the input point cloud in order to reduce undesirable data. Since the objects are all placed on a flat surface of known size and location, it is easy to identify the portion of the scene of interest and remove the rest.

2. Plane Segmentation. The segmentation of normal method, cited in the global pipeline, has been chosen because in the supermarket scenario objects to pick are placed on trolley trays. PCL provides a very useful component to perform this task, called *Sample Consensus Segmentation*. This component is based on the *RANSAC* method, which is a randomized algorithm for robust model fitting. It is used to esti-

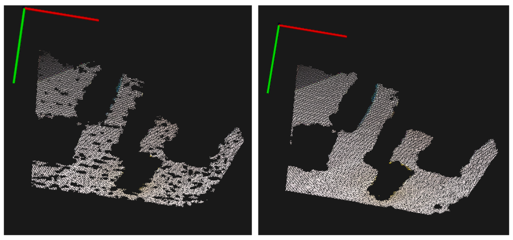

Figure 6: k dependence for the plane segmentation. (a) k=5; (b) k=100.

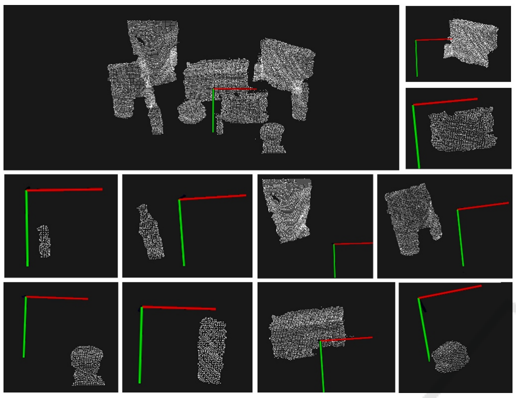

Figure 7: Clustering process.

mate parameters of a mathematical model from a set of observed data that contain both inliers (those points satisfying the model condition) and outliers (all other points). The output of this segmentation process is a vector of *model coefficients*, which are used to show the contents of the inlier set. Note that extracting the plane strongly depends on the quality of the surface normals, as shown in Figure 6. The image on top-left of Figure 7 illustrates the outcome of this step.

3. Objects clustering. The final step of the segmentation process is the *clustering*, that means categorize objects of the scene. The task uses the *Euclidean Cluster Extraction* approach: assuming that a *Kd-tree* structure is used for finding the nearest neighbors, it is needed to fix a threshold d_t, which indicates how close two points are required to belong to the same object. By selecting d_t, the clusters reported in Figure 7 are obtained from the scene.

4. Data Pre-processing. Before the descriptor analysis, as already done for the object models, each cluster is passed through the MLS filter, to improve the quality of the geometric descriptor.

5. VoxelGrid Filter Downsampling. To apply the local FPFH descriptor, a simple downsampling step through a Voxelized Grid approach has been used as a keypoint extraction method. Because model and scene can be provided by different data sources, as seen in Section 2.2, this step makes them more similar and improves the consistency between the model descriptor of an object and the descriptor of the respective cluster, by providing a priori knowledge of the point cloud density. Furthermore, downsampling reduces computational cost.

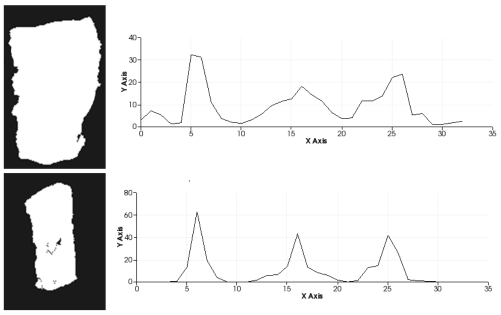

Figure 8: FPFH descriptors of two objects in the set.

6. FPFH Descriptors. Several experiments with different descriptors have been carried out and the FPFH local descriptor has been selected for its robustness. Global descriptors like VFH, ESF or PFH have been analyzed but everyone suffers from some of the specific application requirements. Although the performance of these global descriptors, in ideal operating conditions as described by their authors, represents a good solution to solve the object recognition problem, the following factors have led to the selection of a local descriptor:

- the scenarios are complex in the sense that they contain many objects also similar to each other;
- the objects can be distant from the camera up to two times the ideal distance of 0.5 m defined in the ideal operating conditions (see Section 2.3.4);
- the objects are very often occluded;

FPFH features represent the surface normals and the curvature of the objects, as shown in Figure 8.

7. Point clouds initial alignment: OPRANSAC. Given two generic S_{source} and S_{target} point clouds in 3D space, to be compared they need to be aligned, that means to calculate the rigid geometric transformation to be applied to S_{source} to align it to S_{target}. In this work, an initial alignment is obtained by following the approach in (Buch et al., 2013), i.e., the *Prerejective RANSAC*. This method uses the local FPFH descriptors as the parameters of the consensus function, it finds inliers points and finally it provides the estimated geometric transformation. This alignment is calculated without having previous knowledge about the position or orientation of the target object. To setup the alignment process, the class *SampleConsensusPrerejective* has been used, which implements an efficient RANSAC pose estimation loop.

The following difficulties have been encountered during this phase: in some similar scenes in which the objects on the table were slightly moved, the SoA algorithm did not correctly recognize the model object, often confusing it with objects of different geometry. When it recognized the model, the correspondence rates were very different from one scene to another or similar for different objects. So, the results obtained by these common techniques did not meet the supermarket scenario requirements. This is why a careful analysis of this crucial step has been carried out in order to identify only the most sensitive parameters that affect the algorithm result. The critical parameter that has been identified is the *number of nearest features* to use (γ): small changes generate very different outputs. Then, the objective was to try to select a single value of this parameter for every observed scene and for every object model but all attempts were vain. The adopted solution is to maximize the following fitness function over γ:

$$[I,H] = RANSAC(S_{source}, S_{target}, \gamma) \tag{1}$$

$$fitness(\gamma) = \frac{|I|}{|S_{source}|}, \tag{2}$$

where $|I|$ is the cardinality of the set I of inliers points between the two point clouds S_{target} and S_{source} after the *RANSAC* alignment calculated by using the current value of γ, and H is the 4×4 homogenous transformation matrix to perform such alignment.

In order to maximize the fitness function, two nested loops have been implemented. The inner one computes the best γ variable by increasing it each time of a fixed step (i.e., $\delta_\gamma = 5$). The external one executes this operation for each target cluster $S_{target}[j]$ labelled in the specific scene, i.e., with j from 1 to the number of clusters identified in the scene. Finally, the best result is chosen: the corresponding homogenous transformation matrix and the labelled cluster are selected. This approach has provided surprising and robust results and it has been called *OPRANSAC* to underline the optimization process. The pseudo-code is reported in Algorithm 1.

The maximum fitness value, equal to 1, is obtained when all the points have a near distance below the fixed δ_{th} threshold. The partiality of the views (clusters) and therefore of the point clouds makes unlikely an high level of fitness, although over 70% of matching in the experimental tests have been found. The definition of the similarity parameter therefore allows to compare incomplete objects and models but also it allows to define an optimization heuristics based on the cardinality of the point clouds. Figure 9 shows some results.

8. ICP. Finally, the *ICP* algorithm is applied to refine the estimated 6-DoF object pose. Figure 10 illustrates its output.

Algorithm 1: OPRANSAC initial alignment.

```
 1: input:
 2: $S_{source} \leftarrow$ model point cloud to identify
 3: $S_{target} \leftarrow$ vector of all labelled clusters
 4: $\gamma_0 \leftarrow$ initial value of the critical parameter $\gamma$
 5: $N \leftarrow$ number of iteration for internal loop
 6: $\delta_\gamma \leftarrow$ fixed step for the critical parameter
 7: procedure PERFORM ALIGNMENT
 8:     $fitness = 0$
 9:     $H = I_{4\times4}$
10:     $label = 0$
11:     for $j = 1$ to $S_{target}.size$ do
12:         $\gamma = \gamma_0$
13:         for $i = 1$ to $N$ do
14:             $[I, H_{temp}] = RANSAC(S_{source}, S_{target}[j], \gamma)$
15:             $fitness_{temp} = |I|/|S_{source}|$
16:             if $fitness_{temp} > fitness$ then
17:                 $fitness = fitness_{temp}$
18:                 $H = H_{temp}$
19:                 $label = j$
20:             $\gamma += \delta_\gamma$
```

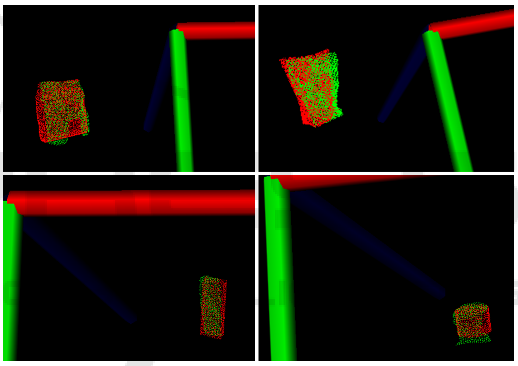
Figure 9: Coarse alignment: cluster (green) and OPRANSAC result (red).

2.3.4 Tests and Performance Assessment

In this subsection the most interesting results obtained by testing the proposed algorithm will be discussed.

Camera Placement. Camera placement depends on three factors. Camera height influences both plane segmentation and object clustering processes. The higher it is placed, the better is the plane segmentation, however the worse is the object clustering. Camera distance from the scene affects the dimensions of the clusters and the dimensions of the captured scene. The larger is the distance, the smaller are the object clusters and the corresponding point clouds have fewer points. On the other hand, to frame as many objects as possible the distance should be large enough. Finally, the distance should high enough to let the camera stay out of the robot workspace so as to avoid an additional obstacle for the pick and place process. As a trade off among the discussed factors,

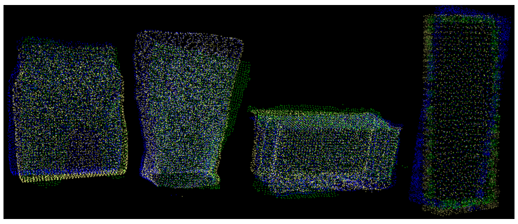
Figure 10: Refined alignment: ICP (yellow) adjusts the OPRANSAC (blue) alignment on the cluster (green).

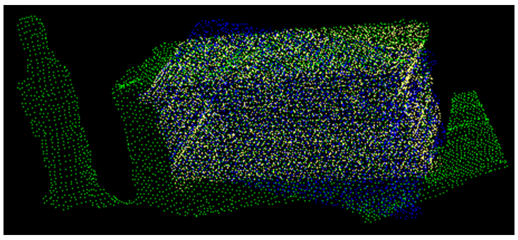
Figure 11: Good alignment with an incorrect clustering (objects too close).

the best distance range of the camera with respect to the objects is between 0.30 m and 0.90 m.

Object Placement. Other relevant aspects are the distance among objects and their placement on the tray. In this work objects are assumed to be randomly placed but all upright on the tray and at a minimum distance of 0.3 m, which is quite critical for a successful collision free motion planning of the grasp phase (see Section 3.2). However, tests with shorter distances have been demonstrated that the recognition phase has still good results as in the example shown in Figure 11, where a cluster erroneously contains two objects but the *OPRANSAC* alignment algorithm correctly aligns the model to the right part of the cluster.

Analysis of the Execution Time. Several experiments have been done to measure the execution times and to evaluate the performance of the recognition algorithm. Table 1 shows the main parameters settings. Then the execution time of the two main phases of the algorithm is calculated, based on an observed scene containing 11 objects. The data, expressed in seconds, are reported in Table 2. Note that the OPRANSAC step requires more computational time due to the introduction of the N-loop for each cluster. The refinement ICP phase shows a constant trend around 700 milliseconds, which is irrelevant.

Confusion Matrix. To evaluate the behavior of the proposed algorithm in terms of its precision and reliability during the object classification, an extensive test has been executed, where the known objects are randomly placed on a tray as explained above. The *confusion matrix* (Table 3) related to twenty different scenes shows the recognition rate of the proposed algorithm. It is important to remark that with-

Table 1: Alignment parameters settings.

OPRANSAC	
ransac_max_iter	50000
ransac_inlier_fraction	0.25
ransac_num_samples	3
ransac_similarity_thresh	0.9
ICP	
icp_max_corr	0.01
icp_out_thresh	0.01
icp_max_iter	50000

Table 2: Execution times (in seconds).

	min	**max**	**mean**
OPRANSAC	31.25	134.7	75.7
ICP	0.5	1.4	0.7

out a criterion to exclude uncertain recognitions, objects are always recognized and this can produce a high value of false positives. A simple way to reduce this phenomenon is to fix a threshold, δ_{fit}, to exclude the cases of poor likeness. This alternative method improves also the execution time of the algorithm because the expected loop is interrupted if the average model-cluster correspondence is lower than δ_{fit}. For each test, the algorithm is invoked, taking the model of the object to be recognized as input. The algorithm output is a selected cluster with a fitness value, *fitness*. By comparing *fitness* with δ_{fit}, it is possible to choose if the correspondence is acceptable or not: if $fitness > \delta_{fit}$, the model-cluster association is considered valid (1), otherwise no (0). Table 3 reports the percentage results by repeating this test for all object models in the same scene and for twenty different scenes. The values in the last column correspond to the cases of failed recognition ($fitness < \delta_{fit}$).

The C, D, F boxes have a higher number of hits because their fitness match values are always the highest for their respective clusters than that with the other clusters, and so the percentage of failure when the aim is to recognize these objects is low. However, they are the objects with simpler geometry and large surface extension, and this means that their point clouds clusters have obviously more samples than those of the others objects. On the opposite side, the clusters of the G, H, I, J objects have fewer points because they are small items and also their distance from the camera cause very coarse and distorted clusters. This limits the fitness values and therefore the success of the algorithm. The curvatures of the smaller objects are not well defined in the clusters and even the filtering is not enough to represent them better. So, the result is a low fitness value implying that the desired model is often confused with an incorrect cluster.

By aggregating the data, 220 tests have been carried out: the algorithm has produces 156 true positive and 52 false positives, which correspond to a correct recognition in the 71% of cases and a wrong recognition in the remaining 23%: the remaining 6% of

Table 3: Confusion matrix based on 20 observed scenes (recognition rate%): models (capital letter) and clusters (lowercase letter) as labelled in Figure 2. **UR** indicates unrecognition rates.

	a	**b**	**c**	**d**	**e**	**f**	**g**	**h**	**i**	**j**	**k**	**UR**
A	**50**	10	20	20	0	0	0	0	0	0	0	0
B	0	**90**	0	0	0	10	0	0	0	0	0	0
C	0	0	**100**	0	0	0	0	0	0	0	0	0
D	0	0	0	**100**	0	0	0	0	0	0	0	0
E	0	0	0	0	**60**	0	30	10	0	0	0	0
F	0	0	0	0	0	**100**	0	0	0	0	0	0
G	0	0	0	0	0	0	**60**	40	0	0	0	0
H	0	0	0	0	0	0	20	**70**	0	0	0	10
I	0	0	0	0	0	20	0	10	**60**	0	0	10
J	0	0	0	0	0	0	0	0	40	**30**	0	30
K	0	0	0	0	0	0	0	0	0	30	**60**	10

the cases analyzed did not produce any association at least equal to δ_{fit}.

3 FLEXIBLE MOTION PLANNING

Enabling a robot manipulator to have the perception of its workspace can drastically improve the flexibility of a industrial system. In this context, this work aims not only to design a 3D vision system able to identify the desired object pose, but also a reliable control able to manipulate it in a dynamic scene. The accuracy has to be sufficient to move the object into the robot workspace without causing issues such as damage or errors. This section describes how two main problems have been solved: the planning of unnecessary robot reconfigurations, and the on-line collision avoidance with unexpected and uncertainly placed objects. The first problem has been solved integrating the Stochastic Trajectory Optimization for Motion Planning (STOMP) planner and the *Trac-IK* kinematics solver into the MoveIt! framework used for motion planning. The second problem has been solved with a reactive control strategy based on distributed proximity sensors used to compute in real-time a modification of the planned trajectory to avoid collisions with unexpected objects in the scene.

3.1 Sensory System

The optimal placement of the RealSense camera for the localization and recognition task (see Section 2.3.4) did not allow to frame the whole robot workspace. Thus, a second depth camera, the Microsoft Kinect, after the calibration procedure already described in Section 2.1, has been integrated into the MoveIt! architecture to build the 3D scene reconstruction for robot motion planning.

To better avoid collisions during the robot planned trajectories, e.g., with objects not known or not perfectly modeled in the scene, four proximity sensors have been mounted on the gripper (see Figure 14), along four main directions (top, bottom, right, left). They have been connected to the Arduino Mega 2560 micro-controller through a TinkerKit shield connected to the ROS network via a serial interface.

3.2 Motion Planning Pipeline

Humans use a remarkable set of strategies to manipulate objects, especially in complex scenes. They pick up, push, slide, and sweep objects with their hands and arms to rearrange surrounding clutter. But the robots look the world differently: they move objects through pick-and-place actions, typically grasping objects in fixed points. The aim of this subsection is to develop a smart pipeline for the robotic manipulation planning based on heuristic considerations.

IK Constrained Solution. Trac-IK Solver is an inverse kinematics solver developed by Traclabs that achieves more reliable solutions than commonly available open source IK solvers (Beeson and Ames, 2015). It provides an alternative inverse kinematics solver to the MoveIt! interface and replaces the default KDL solver. During the experimental tests, KDL algorithms, based on Newton's method, had convergence problems due to the presence of joint limits. Instead, Trac-IK merges a simple extension to KDL's Newton-based convergence algorithm, that detects and mitigates local minima due to joint limits by random jumps, and a Sequential Quadratic Programming (SQP) constrained nonlinear optimization approach, which uses quasi-Newton methods that better handle joint limits. By default, the IK search returns immediately when either of these algorithms converges to an answer. For this work, secondary constraints of manipulability are also provided in order to obtain the 'best' IK solution. To avoid unnecessary reconfigurations, virtual joint limits on relevant joints (see Section 4 for more details) have been used to compute the target configuration to keep it as close as possible to the starting configuration.

STOMP Planner. To choose which planner to use, both the planning time and the quality of the trajectories have been analyzed in detail. First of all the default MoveIt! Open Motion Planning Library (OMPL) has been considered. OMPL provides eleven motion planning algorithms, many of which implement different SoA methods (Kalakrishnan et al., 2011). All these planners have been tested, by studying the significant parameters and tuning their values. Some planners are quite slow, while some others are unable to provide a solution. The table in Figure 12a shows the results: only

OMPL Motion Planners	Solution for Motion Planning of Yaskawa?
BKPIECEkConfigdefault	YES
ESTkConfigDefault	FAILED
KPIECEkConfigDefault	YES
LBKPIECEkConfigdefault	FAILED
PRMkConfigDefault	YES
PRMstarkConfigDefault	FAILED
RRTConnectkConfigDefault	YES
RRTkConfigDefault	YES
RRTstarkConfigDefault	FAILED
SBLkConfigdefault	FAILED
TRRTkconfigDefault	FAILED

(a)

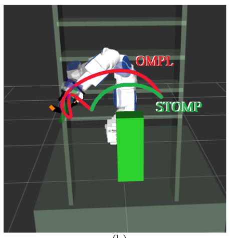

(b)

Figure 12: Typical OMPL planned path Vs STOMP solution.

five of them provided a solution in complex scenarios. In particular, only three planners (*RRTConnectkConfigDefault, RRTkConfigdefault and BKPieceKConfigDefault*) gave good solutions in the shortest planning time.

The conclusion of these tests is that OMPL provides consistent theoretical algorithms but difficult to tune and use effectively in practice. The idea of having a limited number of parameters, which the user is called to define to configure the chosen method, implies that the motion planning management is fully centralized in the algorithm itself and determined by the user in a small part. In these terms, on the one hand this is an advantage but, in practice, the strong stochastic nature of sample-based motion planners has been unsatisfactory because the planners often elaborate unnatural trajectories, as the red planned trajectory in Figure 12b shows. For this reason, a more recent optimal planning algorithm, called STOMP (Kalakrishnan et al., 2011), has been integrated. After hundreds of tests carried out in different environments, the conclusion is that in complex scenes, the STOMP motion planner presents a little longer response time to plan a path, but returns the best natural and smooth trajectories, far enough from the obstacles.

Obstacle Avoidance. The Kinect camera frames the real-time changes of the scene and sends these information to MoveIt! that updates the ROS environment. There are some ROS drivers available to integrate this camera with ROS: this system uses the *openni_kinect* driver, which provides point clouds. The camera is fixed in such a way to cover the robot worksapace as in Figure 1. Figure 13a shows how MoveIt! takes the Kinect depth map as input and publishes a filtered cloud into its RViz environment. This filtered cloud includes the environment around the robot except the robot kinematic chain and everything described as 'collidable' object into the URDF file. The problem is that MoveIt! cannot consider the appearing objects in the scene as obstacles only through the point cloud. For this purpose, it is necessary to create the *3D Occupancy Map* as shown in Figure 13b. The Octomap provides the 3D models in

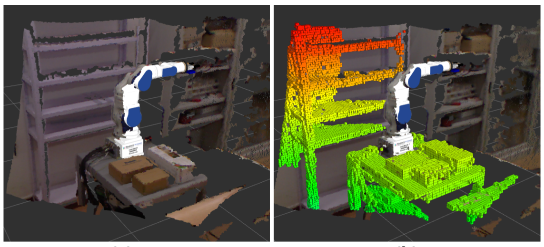

(a) (b)

Figure 13: (a)Point cloud into ROS environment; (b) OctoMap.

the form of volumetric representation of the space and lets the motion planner plans the collision free path. It is a 3D occupancy grid map, based on the octree structure (Hornung et al., 2013).

Among the MoveIt! capabilities, the collision detection is solved through a default collision checking library, called Flexible Collision Library (FCL). FCL supports collision checking for various object types, e.g., OctoMap (Pan et al., 2012).

Task Planning. The implementation of the supermarket scenario task reveals some difficulties, such as:

- the motion planner must have exact knowledge about the robot and its environment;
- every collision that could harm the robot and the environment itself has to be avoided but other collisions are necessary, e.g., when the robot has to get in contact with the graspable object;
- the grasped object has to be considered as an additional part of the robot, hence it should be included in the robot kinematic chain during the motion planning because it possibly increases the size of the end effector;
- it is possible to have additional constraints, such as carrying bottles filled with liquid in an upright position.

A temporal segmentation of the whole task can be a simple solution:

1. **Pre-grasp Phase.** The robot moves from its current configuration to the grasp point neighborhood.
2. **Grasp Phase.** The robot grasps the object.
3. **Manipulation Phase.** The grasped object is raised a few centimeters from its support plane and finally moved till the target point neighborhood.
4. **Release Phase.** The robot reaches the goal location and releases the object.
5. **Retreat Phase.** The robot retreats from the object.

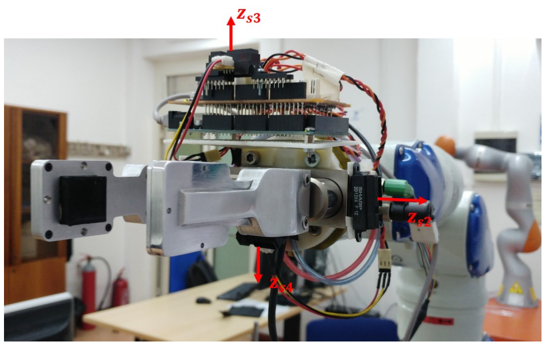

Figure 14: Gripper with proximity sensors (red arrows are the z axes of the sensor frames).

For each subtask, starting from the robot current configuration and given the target pose, the IK is solved by the TracIK solver, which returns to STOMP the target configuration. Finally, STOMP off-line plans the desired trajectory in the joint space, that is $q_d(t)$.

3.3 Reactive Control

Even though the planned arm path is collision-free, the uncertainties on the object locations and the possibility of unseen subjects could lead to unexpected collisions. To counteract these issues, a real-time reactive control algorithm is used at execution time to adapt the planned motion to the actual scene. The method is based on the well-known artificial potential approach (Khatib, 1986) and further developed in (Falco and Natale, 2014) for a mobile manipulator. The planned motion in the joint space $q_d(t)$ is modified on the basis of the distances $d_i, i = 1, \dots, 4$ computed by the four proximity sensors mounted on the gripper as shown in Figure 14. A frame Σ_i is attached to the ith sensor, with an orientation with respect to the robot base frame represented by the rotation matrix $R_{si}(q)$, where q is the current robot configuration. Then a virtual repulsive force applied to the ith sensor is computed as

$$f_i^{si} = \begin{cases} [\ 0 \quad 0 \quad -\alpha/d_i\ ]^T & \text{if } d_{mi} < d_i < d_{Mi} \\ [\ 0 \quad 0 \quad 0\ ]^T & \text{otherwise} \end{cases} \tag{3}$$

being α a suitable gain and d_{mi} and d_{Mi} two thresholds defining the distance range within which the reactive control is active. This repulsive force is then translated into a joint displacement as

$$\delta q = \beta \sum_{i=1}^{4} J_i^T(q) R_{si} f_i^{si}, \tag{4}$$

where $J_i(q)$ is the arm jacobian computed until the ith sensor frame and β is a gain (with the dimensions of a rotational compliance) translating the virtual elastic joint torque $J_i^T(q) R_{si} f_i^{si}$ into a joint displacement. Finally, such displacement is simply added to the planned motion $q_d(t)$, thus endowing the robot with the capability to react to scene uncertainties and dynamics as demonstrated by the experiment presented in the next section.

4 EXPERIMENT

This section describes the execution of a fetch and carry task typical of a shelf refilling process in a supermarket. The robot workspace is shown in Figure 1, with a table and some objects to grasp. Under the assumptions specified in Section 2.2, they are randomly located on the plane and their positions and orientations are not known. The goal of the considered task is to place two objects (labelled as F and K in Figure 2) on the shelving unit, by fixing a target pose very close to other objects already present.

Object Recognition and Localization. After preparing the scene, it is possible to select the specific object to grab. There are two main steps. First of all, an instantaneous frame of the RealSense scene is saved in the form of point cloud. Then, the hybrid pipeline proposed in Section 2.3.3 is called to recognize a specific object, starting from its point cloud model. The algorithm provides the object pose with respect to the robot base represented by the T_{grasp}^{base} homogenous transformation matrix.

Off-line Trajectory Planning. The T_{grasp}^{base} matrix is used to define the picking pose of the end effector. The planning pipeline described in Section 3.2 is sequentially executed. The STOMP planner is invoked at every step. It generates a trajectory by considering the robot current configuration and the target configuration provided by the IK solver. The Trac-IK solver finds a solution which has to be collision-free. If the target pose corresponds to an unreachable or colliding pose, the solver gives up and the task is interrupted. During the tests, the S, E and T joints (see Figure 1) have been identified as the most critical for the robot reconfiguration problem. Two sets of virtual joint limits, one with positive ranges for the selected joint angles and the other negative, have been defined. The IK solver chooses between the two sets according to the signs of the selected joints in the robot current configuration, thus trying to avoid a reconfiguration, e.g., from elbow up to elbow down.

Reactive Control. Octomap has proved to be a rough method to plan collision-free trajectories for tasks that require high accuracy and responsiveness. Unfortunately, it cannot be sufficient. In this experiment, some objects are placed on the shelving unit and the robot is asked to place the grasped object in

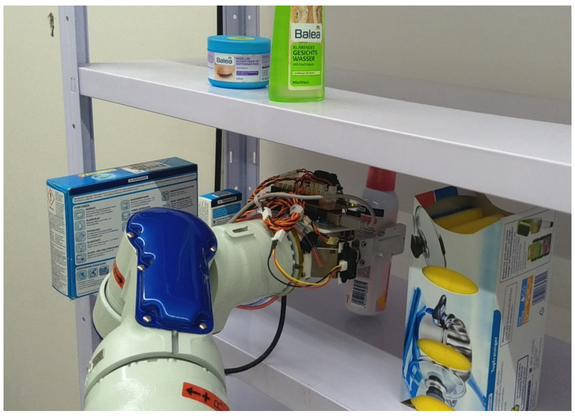

Figure 15: Local trajectory adjustment: place phase.

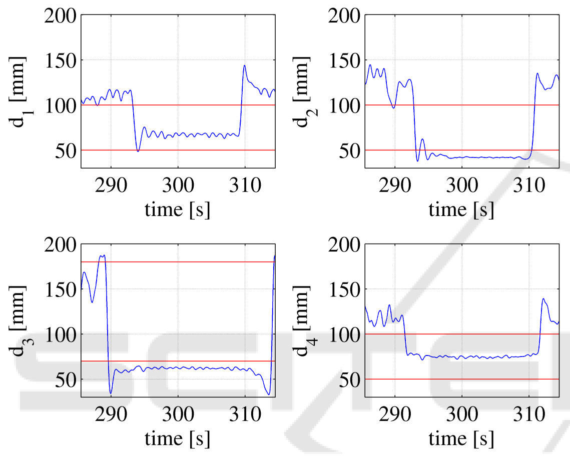

Figure 16: Distances measured by the proximity sensors during the place subtask (thresholds in red).

a position very close to them. The Kinect accuracy is not enough to satisfy the required precision. The use of the proximity sensors can locally correct the planned trajectory, in order to better place the objects. According to this task, the proximity sensors thresholds in (3) are set as follows:

- $d_{m_i} = 50\,\mathrm{mm}$, $d_{M_i} = 100\,\mathrm{mm}$, i=1,2,4
- $d_{m_3} = 70\,\mathrm{mm}$, $d_{M_3} = 170\,\mathrm{mm}$

while the gains are $\alpha = 5\,\mathrm{Nmm}$ and $\beta = 0.3\,\mathrm{rad/Nm}$. The use of proximity sensors has proved to be fundamental during the place phase. As shown in Figure 15 and in the distance signals reported in Figure 16, when the robot end effector enters the shelving unit, the 3rd proximity sensor (with reference to the numbers in Figure 14) detects the upper edge of the shelf, which produces a repulsive downward force applied to the end effector computed as in (3). This force is transformed into joints displacement δq and added to the planned configuration $q_d(t)$ until the specific sensor reads distances into the reactive range, as shown in Figure 17, which reports some planned and

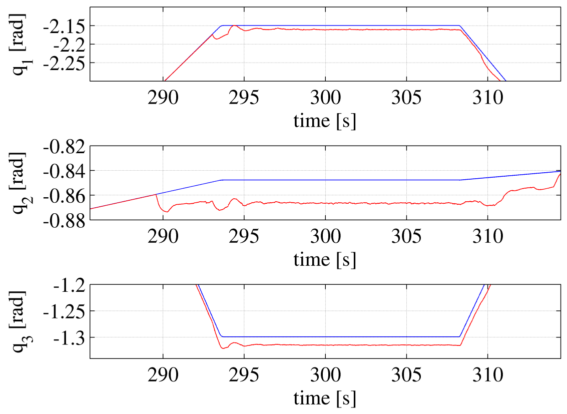

Figure 17: Planned (blue) and actual (red) positions of the first three arm joints.

actual joint positions. Then, the 2nd sensor detects the presence of an obstacle, which produces a repulsive rightward force applied to the end effector. From this moment, the joints displacement δq overlaps the effects of both sensors. Subsequently, the end effector tries to reach the deep target pose following the modified planned trajectory. Thus, even the right object is detected by the 1st sensor. As before, a new repulsive force is generated and the combination of the other two produces a new displacement. In this way, the grasped object is safely placed on the shelf. A video of the complete experiment can be found at the link: https://www.dropbox.com/s/3817sotnno70khp/clip.mp4?dl=0.

5 CONCLUSIONS

This paper presented the implementation of a complete fetch and carry task typical of the in-store logistic scenario, where a large number of different items have to be handled. The proposed methods range from object recognition and localization in cluttered scenes to motion planning and reactive control. Elements of novelty have been proposed in all these technologies that revealed essential for a successful execution of the task in a real setting. Limitations of the approach are mainly due to the perception system for object recognition. The objects are required to be placed at a certain distance from each other and no transparent or thin or polished objects can be handled as it is difficult to reconstruct a good quality point cloud in such cases. Future work will be devoted to integrate the approach with the slipping control strategy by (Costanzo et al., 2018), which aims at enhancing robustness of the task execution.

ACKNOWLEDGEMENTS

This work was supported by the European Commission within the H2020 REFILLS project ID n. 731590 and the H2020 LABOR project ID n. 785419.

REFERENCES

Aldoma, A., Marton, Z.-C., Tombari, F., Wohlkinger, W., Potthast, C., Zeisl, B., Rusu, R., Gedikli, S., and Vincze, M. (2012). Tutorial: Point cloud library: Three-dimensional object recognition and 6 DOF pose estimation. *IEEE Robotics & Automation Magazine*, 19(3):80–91.

Beeson, P. and Ames, B. (2015). TRAC-IK: An open-source library for improved solving of generic inverse kinematics. In *2015 IEEE-RAS 15th International Conference on Humanoid Robots (Humanoids)*, pages 928–935. IEEE.

Bergstrom, N., Bjorkman, M., and Kragic, D. (2011). Generating object hypotheses in natural scenes through human-robot interaction. In *2011 IEEE/RSJ International Conference on Intelligent Robots and Systems*, pages 827–833. IEEE.

Buch, A. G., Kraft, D., Kamarainen, J.-K., Petersen, H. G., and Kruger, N. (2013). Pose estimation using local structure-specific shape and appearance context. In *2013 IEEE International Conference on Robotics and Automation*, pages 2080–2087. IEEE.

Comaniciu, D. and Meer, P. (2002). Mean shift: A robust approach toward feature space analysis. *IEEE Transactions on Pattern Analysis and Machine Intelligence*, 24:603–619.

Costanzo, M., De Maria, G., and Natale, C. (2018). Slipping control algorithms for object manipulation with sensorized parallel grippers. In *2018 IEEE International Conference on Robotics and Automation*. IEEE.

Falco, P. and Natale, C. (2014). Low-level flexible planning for mobile manipulators: a distributed perception approach. *Advanced Robotics*, 28:1431–1444.

Hornung, A., Wurm, K. M., Bennewitz, M., Stachniss, C., and Burgard, W. (2013). OctoMap: An efficient probabilistic 3D mapping framework based on octrees. *Autonomous Robots*, 34:189–206. Software available at `http://octomap.github.com`.

Kalakrishnan, M., Chitta, S., Theodorou, E., Pastor, P., and Schaal, S. (2011). STOMP: Stochastic trajectory optimization for motion planning. In *2011 IEEE International Conference on Robotics and Automation*, pages 4569–4574. IEEE.

Kavraki, L., Svestka, P., Latombe, J.-C., and Overmars, M. (1996). Probabilistic roadmaps for path planning in high-dimensional configuration spaces. *IEEE Transactions on Robotics and Automation*, 12(4):566–580.

Khatib, O. (1986). Real-time obstacle avoidance for manipulators and mobile robots. *Int. J. Rob. Res.*, 5:90–98.

Khokar, K., Beeson, P., and Burridge, R. (2015). Implementation of KDL inverse kinematics routine on the atlas humanoid robot. *Procedia Computer Science*, 46:1441–1448.

Kuffner, J. and LaValle, S. (2000). RRT-connect: An efficient approach to single-query path planning. In *Proceedings 2000 ICRA. Millennium Conference. IEEE International Conference on Robotics and Automation. Symposia Proceedings (Cat. No.00CH37065)*, pages 995–1001. IEEE.

Mishra, A. and Aloimonos, Y. (2011). Visual segmentation of simple objects for robots. In *Robotics: Science and Systems VII*, pages 1–8. Robotics: Science and Systems Foundation.

Muja, M. and Lowe, D. G. (2009). Fast approximate nearest neighbors with automatic algorithm configuration. In *In VISAPP International Conference on Computer Vision Theory and Applications*, pages 331–340.

Nakhaeinia, D., Payeur, P., and Laganiére, R. (2018). A mode-switching motion control system for reactive interaction and surface following using industrial robots. *IEEE/CAA Journal of Automatica Sinica*, 5:670–682.

Pan, J., Chitta, S., and Manocha, D. (2012). FCL: A general purpose library for collision and proximity queries. In *2012 IEEE International Conference on Robotics and Automation*, pages 3859–3866. IEEE.

Papazov, C. and Burschka, D. (2011). An efficient RANSAC for 3d object recognition in noisy and occluded scenes. In *Computer Vision – ACCV 2010*, pages 135–148. Springer Berlin Heidelberg.

Phillips, J. M., Bedrosian, N., and Kavraki, L. (2004). Guided expansive spaces trees: A search strategy for motion- and cost-constrained state spaces. In *2004 IEEE Intl. Conf. on Robotics and Automation*, pages 3968–3973. IEEE.

Rusinkiewicz, S. and Levoy, M. (2001). Efficient variants of the ICP algorithm. In *Proceedings Third International Conference on 3-D Digital Imaging and Modeling*, pages 145–152. IEEE Comput. Soc.

Rusu, R. B., Blodow, N., and Beetz, M. (2009). Fast point feature histograms (FPFH) for 3d registration. In *2009 IEEE International Conference on Robotics and Automation*, pages 3212–3217. IEEE.

Rusu, R. B., Bradski, G., Thibaux, R., and Hsu, J. (2010). Fast 3d recognition and pose using the viewpoint feature histogram. In *2010 IEEE/RSJ International Conference on Intelligent Robots and Systems*, pages 1–4. IEEE.

Rusu, R. B. and Cousins, S. (2011). 3d is here: Point cloud library (PCL). In *2011 IEEE International Conference on Robotics and Automation*. IEEE.

Şucan, I. A. and Kavraki, L. E. (2009). Kinodynamic motion planning by interior-exterior cell exploration. In *Springer Tracts in Advanced Robotics*, pages 449–464. Springer Berlin Heidelberg.

Tombari, F., Salti, S., and Stefano, L. D. (2010). Unique signatures of histograms for local surface description. In *Computer Vision – ECCV 2010*, pages 356–369. Springer Berlin Heidelberg.